SUPPLEMENTARY MATERIAL

The sensitivity of Northern Hemisphere ice sheets to atmospheric forcing during the last glacial cycle using PMIP3 models

Lu NIU, Gerrit LOHMANN, Sebastian HINCK, Evan J. GOWAN, Uta KREBS-KANZOW

The positive degree-day (PDD) scheme

The monthly mean surface air temperature and precipitation are used as input to the ice sheet model. For accumulation, precipitation when temperature is below 0 °C is considered to be snow, and temperature above 2 °C is considered to be rain. For temperatures intermediate of these values, the percentage of snow and rain is linearly interpreted. For ablation, the PDD value is calculated as follows (Calov and Greve, 2005, Eq. 6):

$$PDD = \int_0^A dt \left[\frac{\sigma}{\sqrt{2\pi}} \exp\left(-\frac{T_{\text{mon}}^2}{2\sigma^2} \right) + \frac{T_{\text{mon}}}{2} \operatorname{erfc}\left(-\frac{T_{\text{mon}}}{\sqrt{2}\sigma} \right) \right]. \tag{S1}$$

A random temperature with a normal distribution with a mean value of 0 ("white noise" variation) is added onto the monthly mean temperature at each grid point to account for synoptic variability. The standard deviation σ is 5 K. For the other model parameters, see Table S1.

Ice dynamics

The stress balance computation is a combination of the shallow ice approximation (SIA) and shallow shelf approximation (SSA). SIA and SSA are dominant in grounded and floating ice respectively. Other regions such as ice streams, which have significant internal ice deformation and basal sliding are solved by combing the velocity solution of the two approximations (Winkelmann and others, 2011; Bueler and Brown, 2009).

We use isotropic ice rheology for ice deformation (Paterson, 1994), called the Glen-Paterson-Budd-Lliboutry-Duval flow law (Aschwanden and others, 2012; Lliboutry and Duval, 1985; Paterson and Budd, 1982). Governed by the Glen constitutive law (Glen, 1952; Nye, 1953), ice deformation is temperature dependent, while also a function of pressure and liquid water fraction. A non-dimensional enhancement factor for both SIA and SSA is applied to the flow law. Following the recommendations of Cuffey and Paterson (2010), we set the SIA enhancement factor E_{SIA} to 5. The values of the other parameters and related references are summarized in Table S1. Surface gradients are computed by finite differences to determine the driving stress. The conservation of energy is solved within the ice, the subglacial layer and a layer of thermal bedrock. A geothermal heat flux input is included at the lower boundary. For initialization, the ice temperature is set to the solution of a steady one-dimensional differential equation in which conduction and vertical advection are in balance. The vertical velocity is calculated by linearly interpolating between the surface mass balance rate at the top and zero at the bottom (Aschwanden and others, 2012; The PISM authors, 2016).

The subglacial dynamics

The basal resistance to ice flow is computed based on the hypothesis that a layer of till underlies the ice sheet (Clarke, 2005; Bueler and Brown, 2009). A pseudo-plastic sliding law is used for determining sliding:

$$\vec{\tau}_b = -\tau_c \frac{\vec{u}}{u_{\text{threshold}}^q |\vec{u}|^{1-q}}, \tag{S2}$$

where $\vec{\tau}_b$ is the basal shear stress, τ_c is the yield stress, $\vec{u}$ is the sliding velocity and $u_{\text{threshold}}$ is a parameter called threshold velocity and q is the pseudo-plastic sliding exponent (Table S1).

The Mohr-Coulomb criterion (Cuffey and Paterson, 2010) is used to determine the yield stress τ_c,

$$\tau_c = c_0 + (\tan \phi) N_{\text{till}}, \tag{S3}$$

which is related to the till material property (the till friction angle ϕ) and the effective pressure of the saturated till N_{till}. The till friction angle value, $\phi = 30$ °, is a typical value from lab experiments (Cuffey and Paterson, 2010, p. 268). The till cohesion value, c_0, is set to 0 (Schoof, 2006). The effective pressure, N_{till}, is determined by the following parameterization:

$$N_{\text{till}} = \delta P_o 10^{(e_0/C_c)(1-(W_{\text{till}}/W_{\text{till}}^{\max}))}. \tag{S4}$$

This is based on laboratory experiments on till extracted from an ice stream in Antarctica (Tulaczyk and others, 2000a). P_o is the ice overburden pressure, W_{till} is the effective thickness of water in the till, $W_{\text{till}}^{\max}$ is the maximum amount of water in the till, e_0 is the till reference void ratio, C_c is the till compressibility coefficient and δ is the effective fraction overburden pressure in the till. The water in the base is not conservative in our simulations, it is stored in the till up to the maximum thickness ($W_{\text{till}}^{\max}$). The water exceeding that thickness is drained off instantaneously (Tulaczyk and others, 2000b; Bueler and Brown, 2009).

The ice shelf dynamics

The model for marine portions of ice sheets is from the PIK (Potsdam Institute for Climate Impact Research) component of PISM (Albrecht and others, 2011; Levermann and others, 2012; Winkelmann and others, 2011). The flotation criterion for determining whether the ice floating or grounded is combined with a time-dependent land-sea mask, including relative sea level change. For ice shelf dynamics in PISM, SSA is dominant. The ice shelf calving mechanism is controlled by two schemes. The calving rate is a function of the horizontal strain rates, but the ice shelf is automatically removed when the ice thickness is thinner than the threshold (H_{calthres}) of 200 m.

For the boundary condition at the base of the ice shelf, we follow the setup from Martin and others (2011). The ice at the basal boundary is at pressure melting temperature. The mass flux from ice shelf to ocean is related to the heat flux Q_{heat} between ocean and ice (Martin and others, 2011, Eq. 3-5), which is:

$$Q_{\mathrm{heat}} = \rho_{\mathrm{oce}} c_{\mathrm{poce}} \gamma_{\mathrm{T}} F_{\mathrm{melt}} (T_{\mathrm{oce}} - T_f). \tag{S5}$$

Here, ρ_{oce} is density of ocean water. c_{poce} is specific heat capacity of ocean mixed layer. γ_{T} is the thermal exchange velocity. T_f is a virtual temperature which represent the ocean water freezing temperature at different depths. The ocean temperature, T_{oce}, is set to a constant value of -1.7 °C (Beckmann and Goosse, 2003). F_{melt} is a dimensionless model parameter that we set to 1×10^{-2} to increase the melt rate.

REFERENCES

Adler RF, Huffman GJ, Chang A, Ferraro R, Xie PP, Janowiak J, Rudolf B, Schneider U, Curtis S, Bolvin D, Gruber A, Susskind J, Arkin P and Nelkin E (2003) The version-2 global precipitation climatology project (GPCP) monthly precipitation analysis (1979–present). *J. Hydrometeorol.*, **4**(6), 1147–1167

Albrecht T, Martin M, Haseloff M, Winkelmann R and Levermann A (2011) Parameterization for subgrid-scale motion of ice-shelf calving fronts. *Cryosphere*, **5**(1), 35–44 (doi: 10.5194/tc-5-35-2011)

Aschwanden A, Bueler E, Khroulev C and Blatter H (2012) An enthalpy formulation for glaciers and ice sheets. *J. Glaciol.*, **58**(209), 441–457 (doi: 10.3189/2012JoG11J088)

Aschwanden A, Aøalgeirsdóttir G and Khroulev C (2013) Hindcasting to measure ice sheet model sensitivity to initial states. *Cryosphere*, **7**(4), 1083–1093 (doi: 10.5194/tc-7-1083-2013)

Beckmann A and Goosse H (2003) A parameterization of ice shelf–ocean interaction for climate models. *Ocean Model. (Oxf)*, **5**(2), 157–170

Bueler E and Brown J (2009) Shallow shelf approximation as a "sliding law" in a thermomechanically coupled ice sheet model. *J. Geophys. Res. Solid Earth*, **114**, 1–21 (doi: 10.1029/2008JF001179)

Calov R and Greve R (2005) A semi-analytical solution for the positive degree-day model with stochastic temperature variations. *J. Glaciol.*, **51**(172), 173–175

Clarke GK (2005) Subglacial processes. *Annu. Rev. Earth Planet. Sci.*, **33**, 247–276

Cuffey KM and Paterson WSB (2010) *The physics of glaciers*. Academic Press

Glen J (1952) Experiments on the deformation of ice. *J. Glaciol.*, **2**(12), 111–114

Kalnay E, Kanamitsu M, Kistler R, Collins W, Deaven D, Gandin L, Iredell M, Saha S, White G, Woollen J, Zhu Y, Chelliah M, Ebisuzaki W, Higgins W, Janowiak J, Mo KC, Ropelewski C, Wang J, Leetmaa A, Reynolds R, Jenne R and Joseph D (1996) The NCEP/NCAR 40-year reanalysis project. *Bull. Am. Meteorol. Soc.*, **77**(3), 437–471

Levermann A, Albrecht T, Winkelmann R, Martin MA, Haseloff M and Joughin I (2012) Kinematic first-order calving law implies potential for abrupt ice-shelf retreat. *Cryosphere*, **6**(2), 273–286 (doi: 10.5194/tc-6-273-2012)

Lliboutry L and Duval P (1985) Various isotropic and anisotropic ices found in glaciers and polar ice caps and their corresponding rheologies. In *Ann. Geophys.*, volume 3, 207–224, Gauthier-Villars

Martin MA, Winkelmann R, Haseloff M, Albrecht T, Bueler E, Khroulev C and Levermann A (2011) The Potsdam Parallel Ice Sheet Model (PISM-PIK)–Part 2: Dynamic equilibrium simulation of the Antarctic ice sheet. *Cryosphere*, **5**(3), 727–740 (doi: 10.5194/tc-5-727-2011)

Nye JF (1953) The flow law of ice from measurements in glacier tunnels, laboratory experiments and the Jungfraufirn borehole experiment. In *Proceedings of the Royal Society of London A: Mathematical, Physical and Engineering Sciences*, volume 219, 477–489, The Royal Society

Paterson W (1994) *The Physics of Glaciers*. Butterworth-Heinemann

Paterson W and Budd W (1982) Flow parameters for ice sheet modeling. *Cold Reg. Sci. Technol.*, **6**(2), 175–177

Ritz C (1997) Eismint intercomparison experiment: Comparison of existing Greenland models

Schoof C (2006) A variational approach to ice stream flow. *J. Fluid Mech.*, **556**, 227–251

The PISM authors (2016) PISM, a Parallel Ice Sheet Model

Tulaczyk S, Kamb WB and Engelhardt HF (2000a) Basal mechanics of ice stream B, West Antarctica: 1. Till mechanics. *J. Geophys. Res. Solid Earth*, **105**(B1), 463–481

Tulaczyk S, Kamb WB and Engelhardt HF (2000b) Basal mechanics of ice stream B, West Antarctica: 2. Undrained plastic bed model. *J. Geophys. Res. Solid Earth*, **105**(B1), 483–494

Winkelmann R, Martin MA, Haseloff M, Albrecht T, Bueler E, Khroulev C and Levermann A (2011) The Potsdam Parallel Ice Sheet Model (PISM-PIK) - Part 1: Model description. *Cryosphere*, **5**(3), 715–726 (doi: 10.5194/tc-5-715-2011)

Zhang X, Lohmann G, Knorr G and Xu X (2013) Different ocean states and transient characteristics in Last Glacial Maximum simulations and implications for deglaciation. *Clim. Past*, **9**(5), 2319–2333 (doi: 10.5194/cp-9-2319-2013)

Table S1. Parameters used in our glacial cycle simulations.

Parameter	Name	Value	Unit	Reference
E_{SIA}	SIA enhancement factor	5.0	1	Cuffey and Paterson (2010)
E_{SSA}	SSA enhancement factor	1.0	1	Cuffey and Paterson (2010)
q	Pseudo-plastic sliding exponent	0.25	1	Aschwanden and others (2013)
$u_{\mathrm{threshold}}$	Pseudo-plastic threshold velocity	100.0	$\mathrm{m\,a^{-1}}$	Aschwanden and others (2013)
Φ	Till friction angle	30	$^{\circ}$	Cuffey and Paterson (2010, p. 268)
c_0	Till cohesion	0	kPa	Schoof (2006)
e_0	Till reference void ratio	0.69	1	Tulaczyk and others (2000a)
C_c	Till compressibility coefficient	0.12	1	Tulaczyk and others (2000a)
δ	Till effective fraction overburden	0.01	1	-
$W_{\mathrm{till}}^{\mathrm{max}}$	Maximum amount of water in till	1	m	-
H_{calthres}	Calving ice threshold thickness	200	m	-
T_{oce}	Ocean temperature	-1.7	$^{\circ}$C	(Beckmann and Goosse, 2003)
F_{melt}	Ocean model melt factor	1×10^{-2}	1	-
σ	Standard deviation of the daily temperature	5.0	K	Ritz (1997)
F_{snow}	Positive degree day factor for snow	3.3×10^{-3}	$\mathrm{m\ K^{-1}\ day^{-1}}$	Ritz (1997)
F_{ice}	Positive degree day factor for ice	8.8×10^{-3}	$\mathrm{m\ K^{-1}\ day^{-1}}$	Ritz (1997)
$\theta_{\mathrm{refreeze}}$	Refreezing rate of melted snow	0.6	1	Ritz (1997)

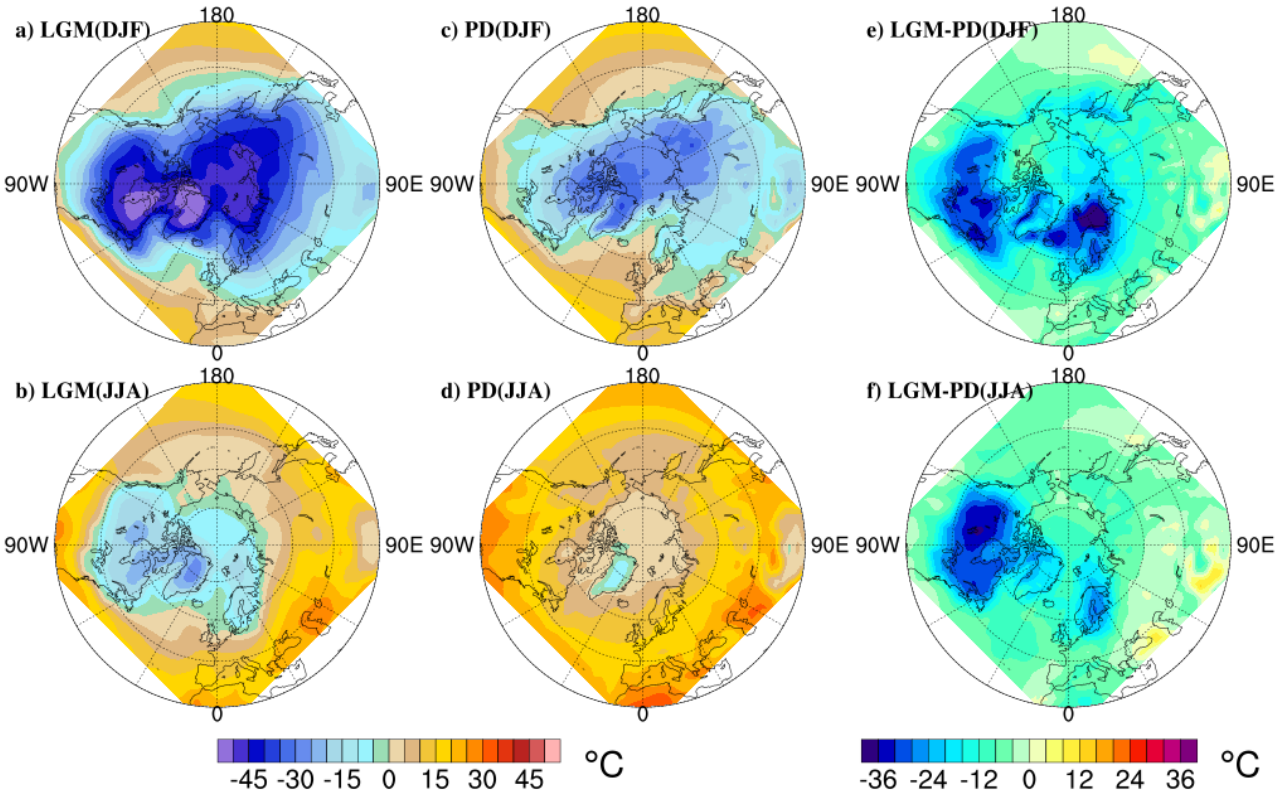

Fig. S1. Winter (DJF) and summer (JJA) surface air temperature for Last Glacial Maximum (LGM, a-b) from COSMOS-AWI (Zhang and others, 2013) and Present Day (PD, c-d) from NCEP Reanalysis data (Kalnay and others, 1996), and the difference between LGM and PD surface air temperature (LGM minus PD, e-f).

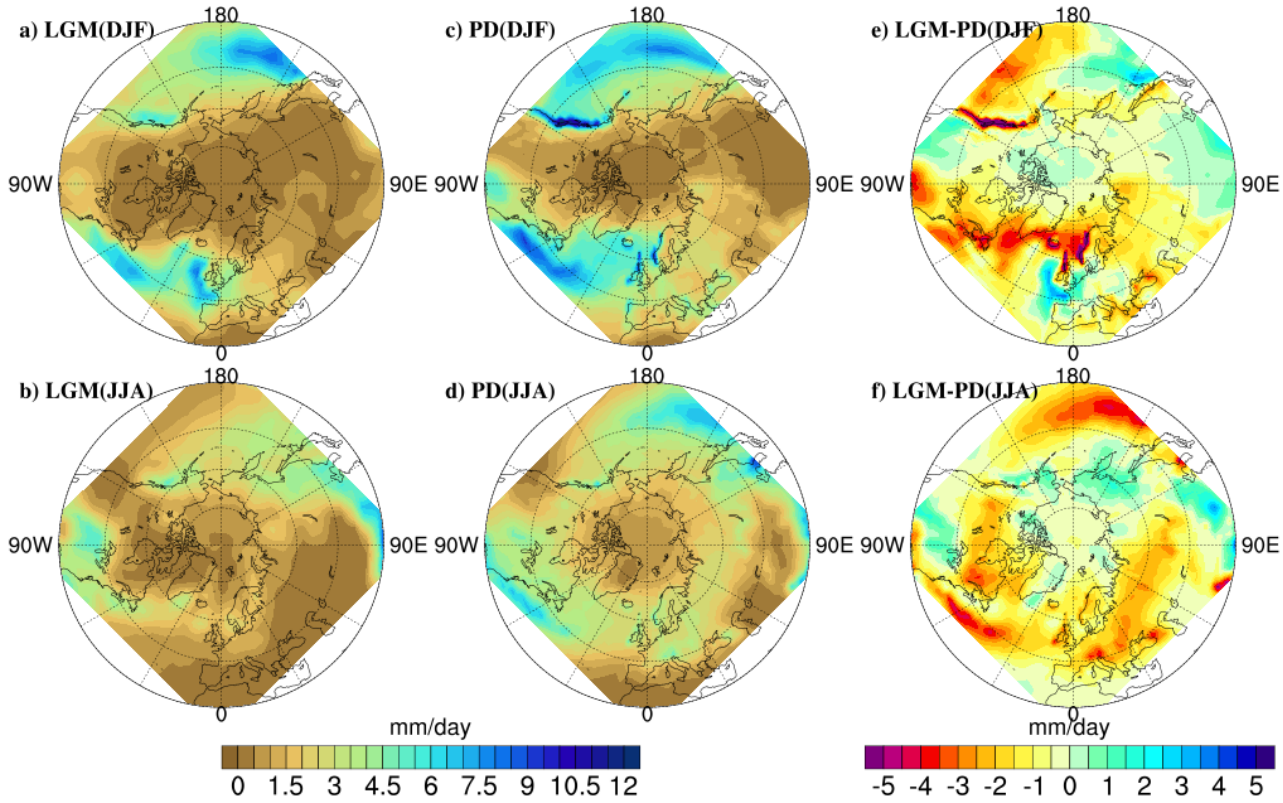

Fig. S2. Same as Fig. S1, but for precipitation. The present day precipitation is from GPCP precipitation products (Adler and others, 2003).

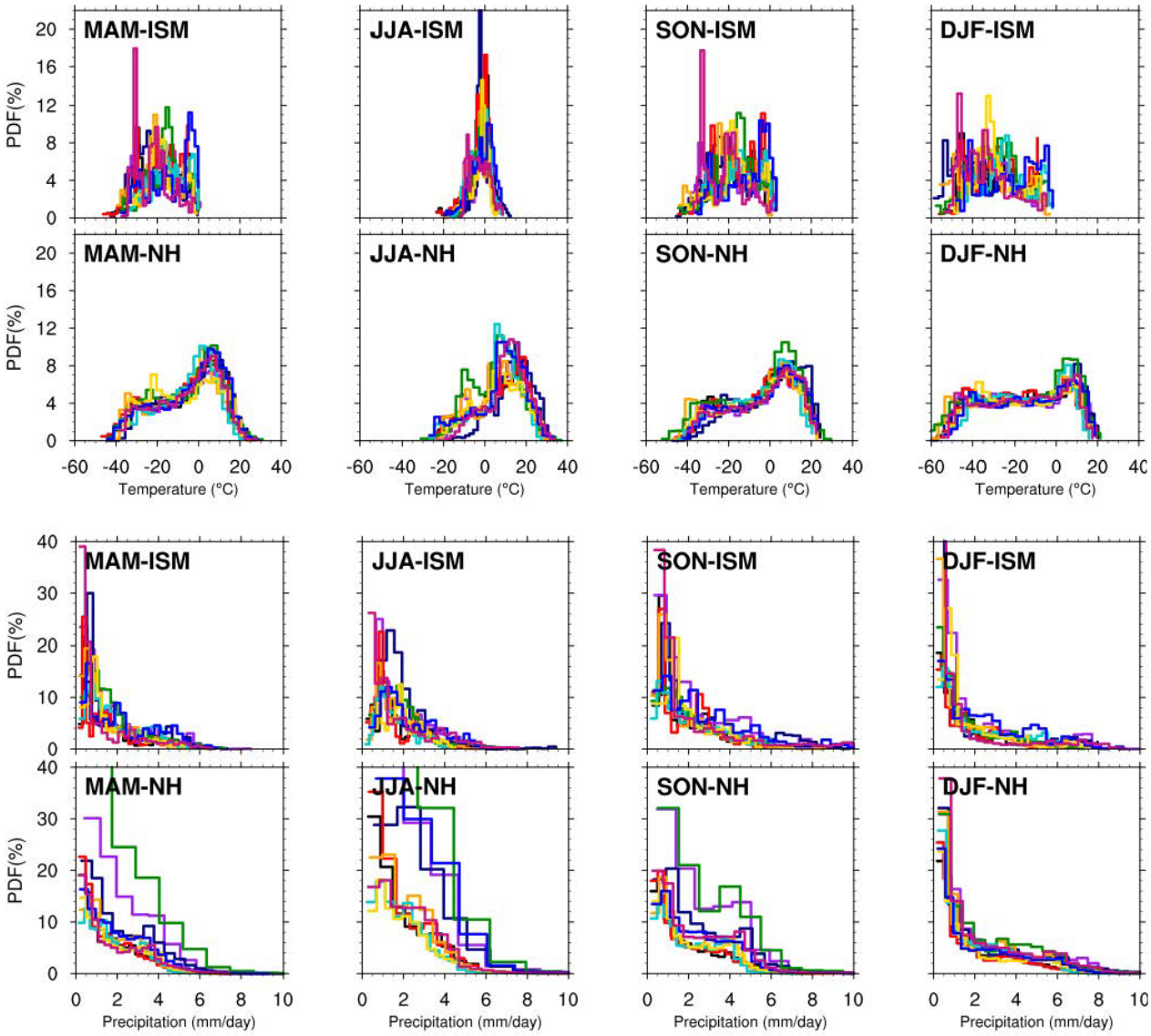

Fig. S3. Probability Distribution Functions (PDF) of surface air temperature (upper two rows) and precipitation (lower two rows) over the ice sheet margins (ISM) and Northern Hemisphere (NH) for different seasons (MAM, JJA, SON, DJF) for different models. For the colors, we refer to Fig. 4 of the main text.

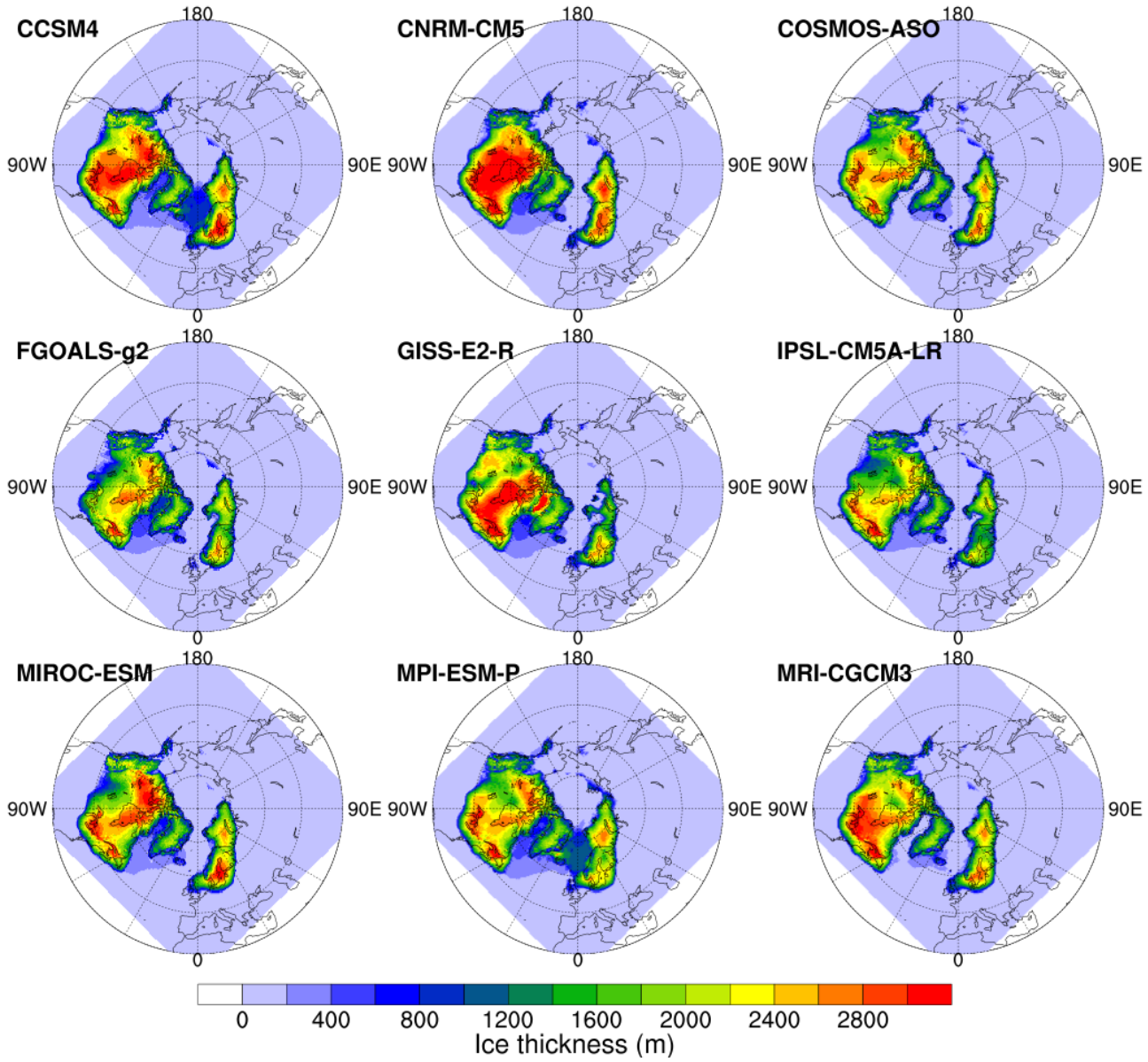

Fig. S4. Modelled ice thickness at the Last Glacial Maximum (LGM, 21 kyr BP) from experiment PMIP3-fixCOSMOSTemp.

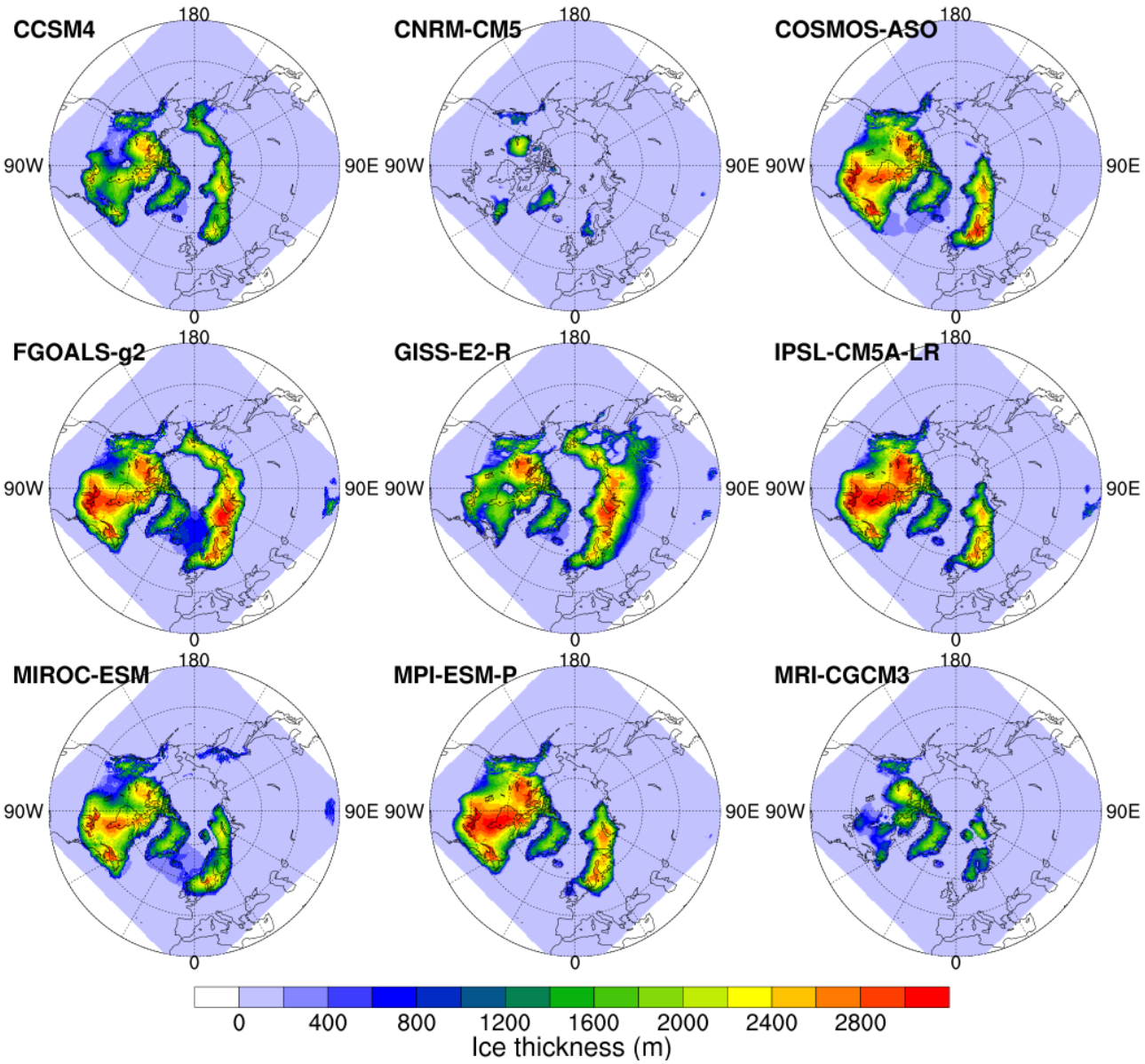

Fig. S5. Same as Fig. S4, except that experiment from PMIP3-fixCOSMOSPrecip.

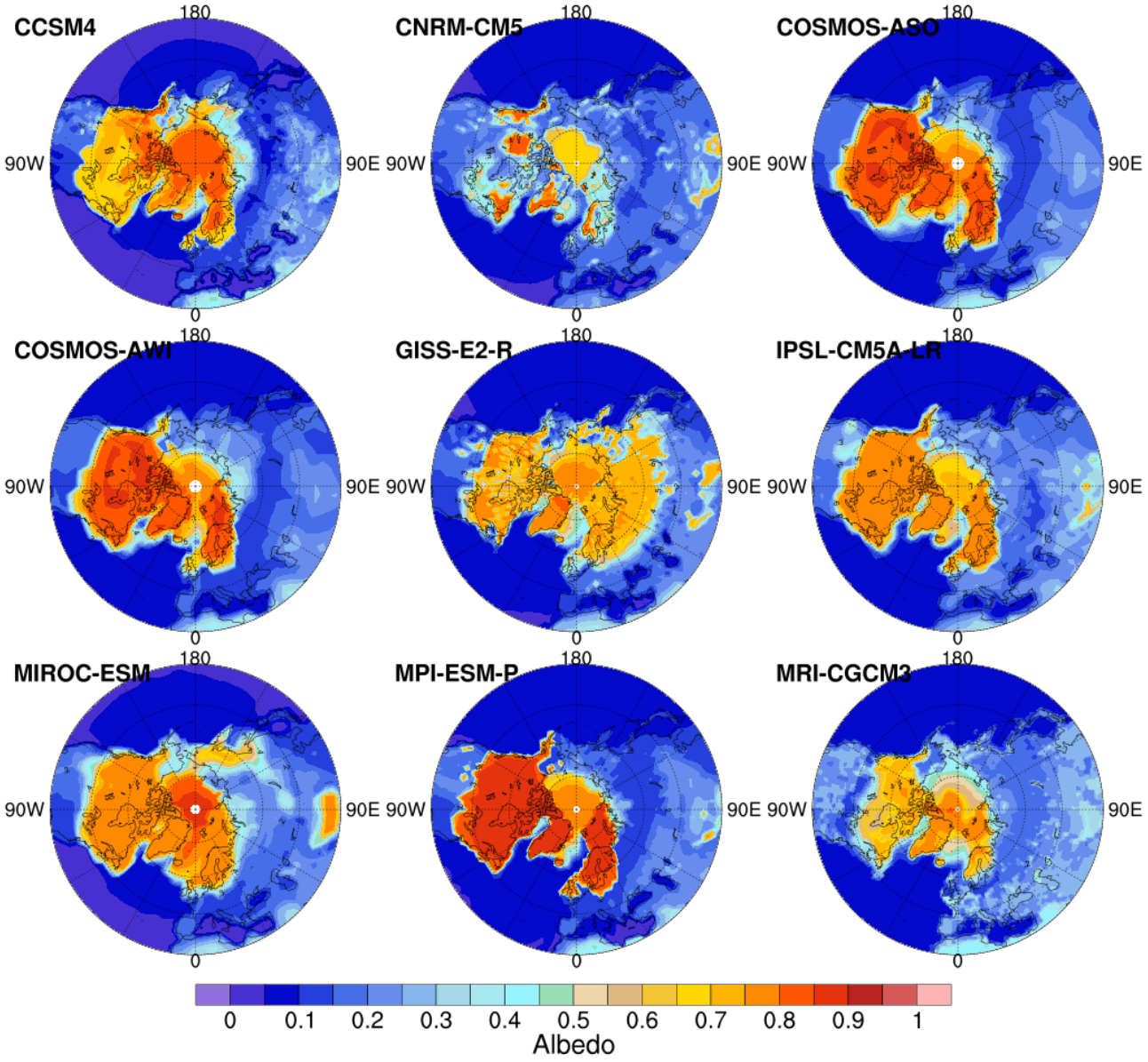

Fig. S6. Surface albedo in summer from different models participating in PMIP3. The albedo is calculated as the ratio of surface upward shortwave radiation and surface downward shortwave radiation. (The shortwave upward radiation for FGOALS-g2 is not available from the PMIP3 data output online.)

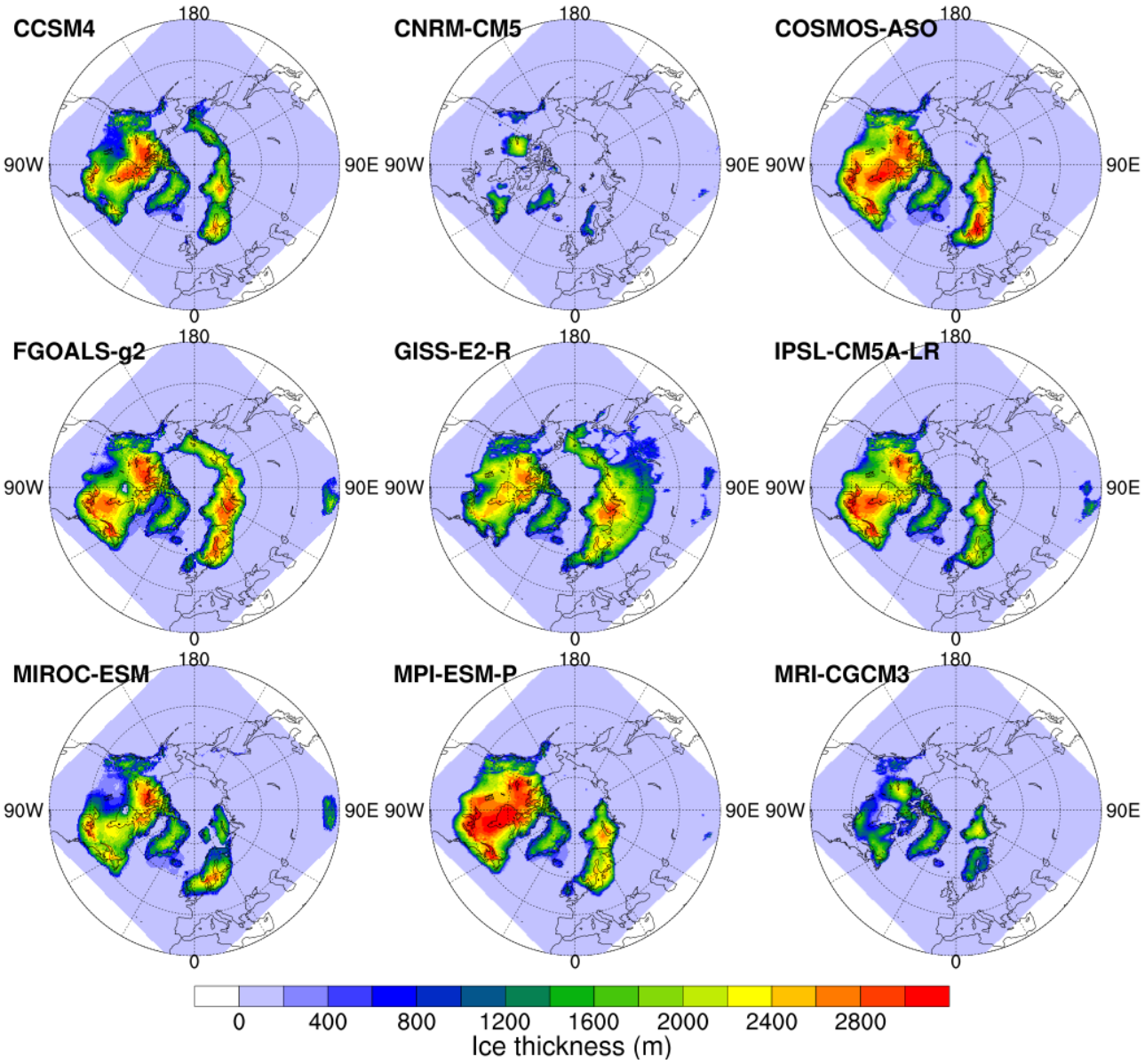

Fig. S7. Same as Fig. S4, except that experiment from PMIP3-PIpmip3.

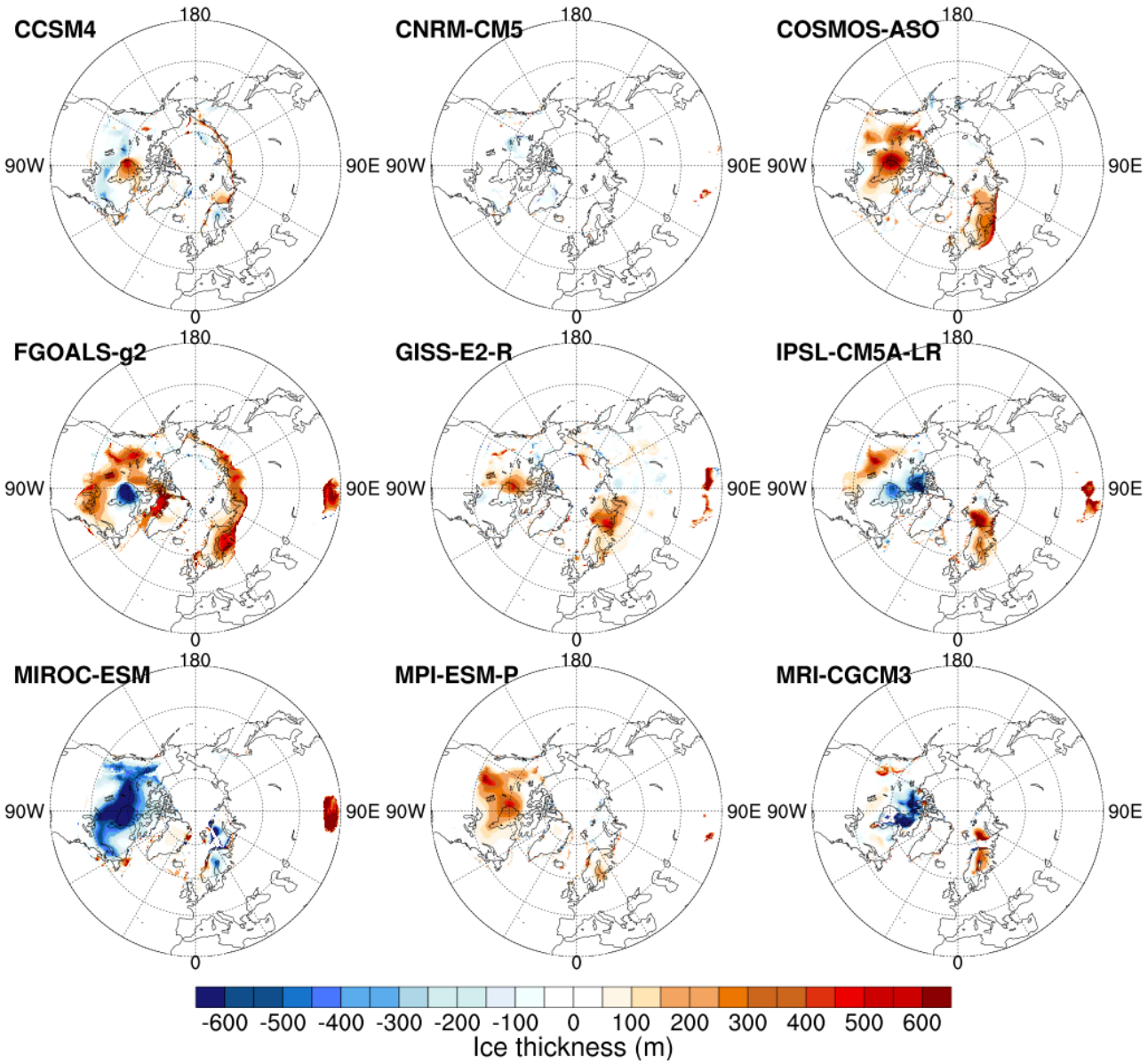

Fig. S8. Simulated ice thickness differences at the LGM between experiments from PMIP3-PDobs and PMIP3-PIpmip3, PIpmip3-PDobs.

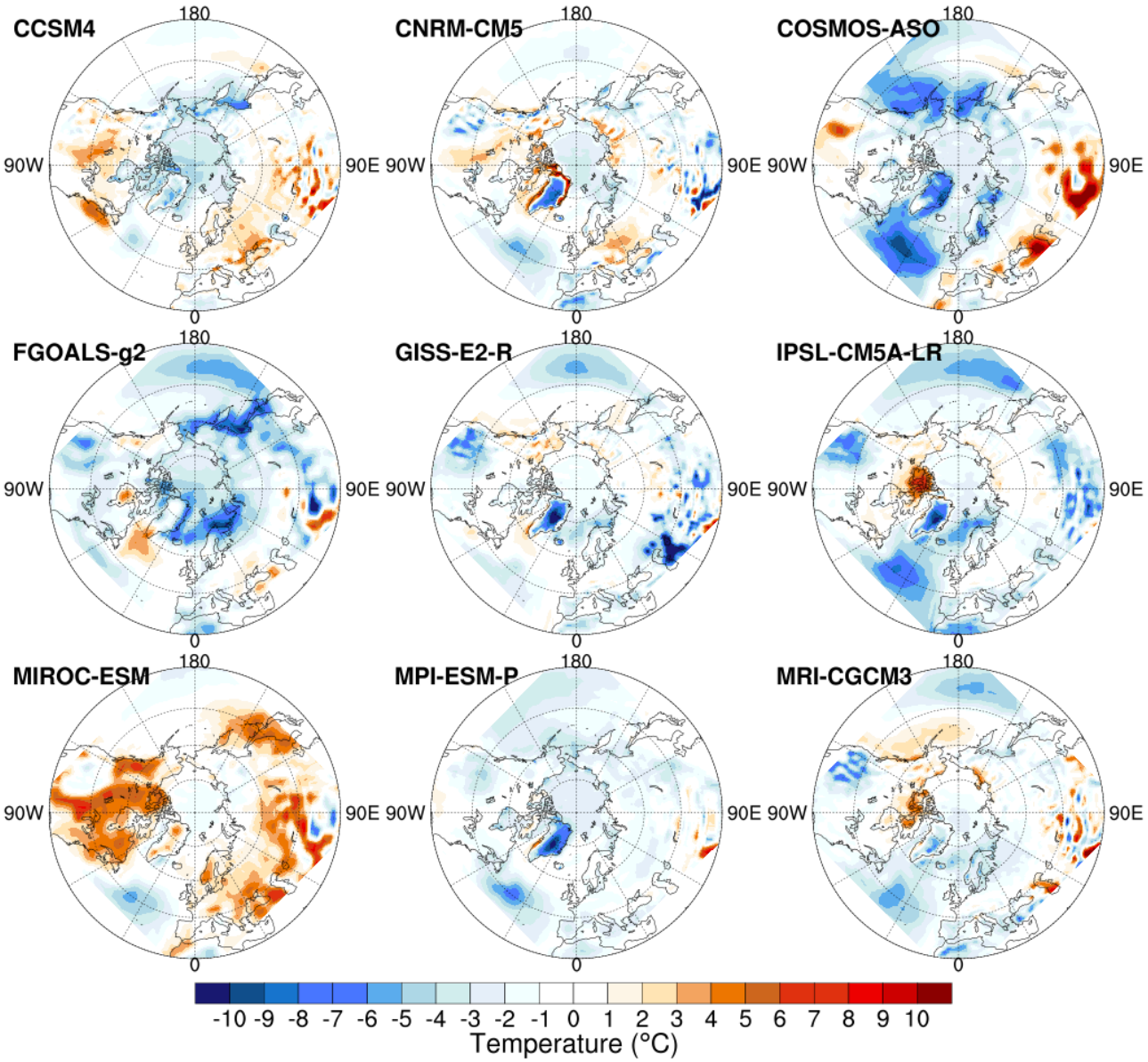

Fig. S9. Summer (JJA) surface air temperature differences at present day between reanalysis products (PDobs) and PMIP3 PI GCM output (PIpmip3), PIpmip3-PDobs.